Original Research

Decreased Brain Stiffness in Alzheimer's Disease Determined by Magnetic Resonance Elastography

Matthew C. Murphy, PhD, John Huston III, MD,* Clifford R. Jack Jr, MD, Kevin J. Glaser, PhD, Armando Manduca, PhD, Joel P. Felmlee, PhD, and Richard L. Ehman, MD

Purpose: To test patient acceptance and reproducibility of the 3D magnetic resonance elastography (MRE) brain exam using a soft vibration source, and to determine if MRE could noninvasively measure a change in the elastic properties of the brain parenchyma due to Alzheimer's disease (AD).

Materials and Methods: MRE exams were performed using an accelerated spin-echo echo planar imaging (EPI) pulse sequence and stiffness was calculated with a 3D direct inversion algorithm. Reproducibility of the technique was assessed in 10 male volunteers, who each underwent four MRE exams separated into two imaging sessions. The effect of AD on brain stiffness was assessed in 28 volunteers, 7 with probable AD, 14 age- and gender-matched PIB-negative (Pittsburgh Compound B, a PET amyloid imaging ligand) cognitively normal controls (CN–), and 7 age- and gender-matched PIB-positive cognitively normal controls (CN+).

Results: The median stiffness of the 10 volunteers was 3.07 kPa with a range of 0.40 kPa. The median and maximum coefficients of variation for these volunteers were 1.71% and 3.07%. The median stiffness of the 14 CN– subjects was 2.37 kPa (0.44 kPa range) compared to 2.32 kPa (0.49 kPa range) within the CN+ group and 2.20 kPa (0.33 kPa range) within the AD group. A significant difference was found between the three groups ($P = 0.0055$, Kruskal–Wallis one-way analysis of variance). Both the CN+ and CN– groups were significantly different from the AD group.

Conclusion: 3D MRE of the brain can be performed reproducibly and demonstrates significantly reduced brain tissue stiffness in patients with AD.

Key Words: Alzheimer's disease; MR elastography; brain; stiffness
J. Magn. Reson. Imaging 2011;34:494–498.

Department of Radiology, Mayo Clinic College of Medicine, Rochester, Minnesota, USA.

Additional Supporting Information may be found in the online version of this article.

Contract grant sponsor: National Institutes of Health (NIH); Contract grant numbers: R01 EB001981 and AG11378..

*Address reprint requests to: J.H., 200 First St. SW, Rochester, MN 55905. E-mail: jhuston@mayo.edu

Received October 29, 2010; Accepted June 6, 2011.

DOI 10.1002/jmri.22707
View this article online at wileyonlinelibrary.com.

ALZHEIMER'S DISEASE (AD) is characterized clinically by the progressive impairment of specific cognitive functions including memory, language, motor skills, and perception. Pathologically, AD demonstrates the accumulation of extracellular amyloid plaques, intracellular neurofibrillary tangles, and neurodegeneration (1). Due to changing demographics, the disease is expected to dramatically increase in prevalence in the U.S. population, growing from 4.5 million people with AD today to an estimated 13.2 million by 2050 (2). Improved treatment could mitigate the impact of the predicted increase in AD prevalence, and that treatment would be aided by earlier and more sensitive detection of the disease.

Magnetic resonance elastography (MRE) is an emerging technique capable of noninvasively and quantitatively measuring tissue stiffness (3). MRE is a three-step process beginning with the induction of shear waves in the tissue to be examined via an external source of vibration. Second, the shear waves are imaged with a phase-contrast MRI pulse sequence with motion-encoding gradients synchronized with the applied vibration. Finally, the images of the wave motion are inverted to calculate the tissue stiffness. MRE is analogous to manual palpation, which has a long history in the practice of medicine as a clinical diagnostic tool for examining tissues such as the breast and thyroid for focal and diffuse diseases. In fact, MRE of the liver has already matured to a point where it is replacing needle biopsies for the diagnosis of fibrosis and cirrhosis in a growing number of clinical practices (4).

Performing MRE of the brain has presented unique technical challenges, including the introduction of shear waves through the bony calvarium as well as performing efficient sampling and processing of a 3D displacement field. We have developed a soft "pillow-like" vibration source to produce intracranial shear waves and implemented an accelerated spin-echo echo planar imaging (EPI) sequence allowing fast volumetric acquisitions that fully sample the required extent of *k*-space.

The purpose of this work was to test the patient acceptance and reproducibility of the 3D MRE brain exam using the soft vibration source, and to determine if MRE could noninvasively measure a change in the elastic properties of the brain parenchyma due to AD.

SUBJECTS AND METHODS

Subject Recruitment

These studies were reviewed and approved by our Institutional Review Board. The subjects were recruited and imaged after obtaining written informed consent.

To test the technique's reproducibility, 10 male volunteers all without known neurological diseases were recruited with a median age of 29 years (range, 25–52 years). MRE was performed on each individual a total of four times in two sessions separated by an average of 8.7 days (range, 4–20 days). On each day a complete MRE exam was performed and then the patient was removed from the MRI table and the actuator components were disassembled. Subsequently, the equipment and subject were again positioned on the MRI table and a second complete MRE exam was performed.

To examine the effect of AD on brain stiffness, 28 subjects were recruited including 7 with probable AD, 14 age- and gender-matched Pittsburgh Compound B (PIB)-negative cognitively normal controls (CN−) and 7 age- and gender-matched PIB-positive cognitively normal controls (CN+). All subjects were identified from the Mayo Clinic Study of Aging (MCSA) and Alzheimer's Disease Patient Registry (ADPR) database. All subjects recruited into the ADRC and ADPR are followed prospectively. Criteria for the diagnosis of cognitively normal controls were: 1) no active neurologic or psychiatric disorders; 2) any ongoing medical problems or their treatments did not interfere with cognitive function; 3) a normal neurological exam; 4) no psychoactive medications; and 5) were independently functioning community dwellers. The diagnosis of probable AD was made according to the Diagnostic and Statistical Manual for Mental Disorders, III Edition–Revised (DSM-III-R) Criteria for dementia, and National Institute of Neurological and Communicative Disorders and Stroke/Alzheimer's Disease and Related Disorders Association Criteria (NINCDS/ADRDA) for AD. PIB is the most widely studied PET amyloid imaging ligand to date. Approximately one-third of cognitively normal elderly subjects harbor a significant amyloid plaque load, one of the cardinal pathological features of AD (5). As part of the MCSA and ADRC studies, all subjects had already undergone brain amyloid imaging with PIB to establish the presence or absence of Aβ brain amyloid. Subjects with a global cortical PIB score of less than 1.5 (the ratio of uptake in the cortex versus a cerebellar reference region of interest [ROI]) were considered PIB-negative, while scores above 1.5 were considered PIB-positive (6). The median age of the CN− group was 81.5 (range, 75–89), the median age of the CN+ group was 83 (range, 73–93), and the median age of the AD group was 85 (range, 76–94) ($P = 0.17$, Kruskal–Wallis). The CN− group consisted of ten men and four women while the CN+ and AD groups consisted of five men and two women.

MRE

MRE data were collected with a single-shot spin-echo EPI pulse sequence on a 3.0T MR imager (SIGNA Excite, GE Healthcare, Waukesha, WI). Shear waves were introduced into the brain through a soft pillow-like vibration source using a pneumatic actuator. The active component of the actuator, located outside of the scan room, was comprised of a waveform generator, an amplifier, and an acoustic speaker. The passive pillow-like component consisted of a soft, inelastic, fabric cover over a porous, springy, mesh measuring 15 × 9 × 1.5 cm. The soft vibration source was placed under the subject's head within an 8-channel receive-only head coil. The active and passive driver components were connected by a 24-foot long, 0.75-inch diameter flexible tube from the active driver terminating in a 0.5-inch diameter, 1.5-foot long tube integrated into the passive driver.

For the reproducibility experiments the driver system was operated at 55 Hz and the resulting tissue motion was imaged with the EPI MRE imaging sequence using the following parameters: axial slices, TR/TE = 1636/64.0 msec, field of view (FOV) = 25.6 cm, bandwidth (BW) = ± 250 kHz, 60 × 60 imaging matrix reconstructed to 64 × 64, 3× ASSET acceleration, 2.5-mm thick slices with a 1.5-mm skip, one 4-G/cm 18.2-msec zeroth- and first-order moment nulled motion-encoding gradient on each side of the refocusing radiofrequency (RF) pulse synchronized to the motion, motion encoding in the positive and negative x, y, and z directions, and four phase offsets sampled over one period of the 55-Hz motion.

For the study of AD the driver system was operated at 60 Hz and the resulting tissue motion was imaged with the EPI MRE imaging sequence using the following parameters: axial slices, TR/TE = 1500/61.3 msec, FOV = 25.6 cm, BW = ± 250 kHz, 60 × 60 imaging matrix reconstructed to 64 × 64, 3× ASSET acceleration, 2.5-mm thick slices with a 1.5-mm skip, one 4-G/cm 18.2-ms zeroth- and first-order moment nulled motion-encoding gradient on each side of the refocusing RF pulse synchronized to the motion, motion encoding in the positive and negative x, y, and z directions, and four phase offsets sampled over one period of the 60-Hz motion. A second MRE scan of ≈1.5 minutes was performed with the motion source turned off sampling only two phase offsets 90° apart to provide additional data for the signal-to-noise ratio (SNR) calculations. The resulting images had isotropic 4-mm resolution and required at most a 3.5-minute total acquisition time.

Image Processing

Eighteen slices covering the cerebrum were used for image processing in all subjects. The first temporal harmonic of the vector curl of the wave data was calculated from the phase images to remove contributions from longitudinal wave propagation and static phase errors (7). The spatial derivatives were calculated using central differences over a 3 × 3 × 3 window. The first-harmonic curl data were prefiltered with a 3 × 3 × 3 filter of the form $(1-x^2)^2(1-y^2)^2(1-z^2)^2$ where $-1 \leq x, y, z \leq 1$ (8), and inverted with a 3D direct inversion (DI) algorithm (9). The median stiffness for each individual was reported from a global ROI. For display purposes, the elastograms were filtered with a 3 × 3 × 3 median filter.

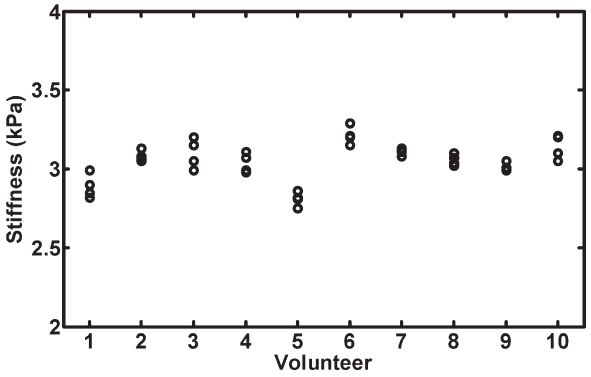

Figure 1. Summary plot of reproducibility results. Each marker represents the median stiffness for a separate MRE exam. Each subject underwent four exams over 2 days. Each subject displays a tight distribution of stiffness measurements, all with a coefficient of variation less than 3.1%.

For the reproducibility experiments the ROI used for reporting the median tissue stiffness included the whole brain excluding 3 voxels from the edge of the calvarium (≈1/3 of the shear wavelength), the longitudinal fissure, the ventricles, and low signal magnitude regions such as the midbrain.

For the AD experiments the curl calculation as described above was also performed on the data acquired with the motion turned off. The standard deviation of the no-motion curl data in $3 \times 3 \times 3$ sliding windows was used as an estimate of the local noise of the curl data. The local SNR of the curl data was calculated as the pixel-by-pixel ratio of the amplitude of the first-harmonic of the curl data to the noise standard deviation. The ROI utilized to calculate the tissue stiffness included the portion of the brain with SNR > 5, that was at least 3 voxels from the brain surface and the longitudinal fissure to remove edge artifacts, and excluded any voxels with a cerebrospinal fluid (CSF) content greater than 30%. The edge voxels were removed by first thresholding the magnitude images to create a mask of the brain, then manually drawing a line along the longitudinal fissure to create a line of voxels that were removed from all slices, and finally three serial erosions with a $3 \times 3 \times 3$ structural element. CSF content was calculated by segmenting a 3D T1-weighted image as described by Jack et al (5). The magnitude data from the MRE acquisition were registered to the T1 images with a rigid body transformation and the segmented CSF images were resliced to the MRE data to obtain the CSF content for each voxel of the MRE data.

Statistical Analysis

The CN−, CN+, and AD groups were compared using the Kruskal–Wallis one-way analysis of variance. The Wilcoxon rank sum test was used for pairwise comparisons of the groups to determine which were significantly different from one another.

RESULTS

All 40 reproducibility exams were completed successfully and provided data adequate for inversion. The median stiffness for the 10 volunteers was 3.07 kPa (interindividual range: 2.81–3.21 kPa). The results indicated that 3D brain MRE can be performed with a coefficient of variation of 3.1% or less. Summary data for each subject are shown in Fig. 1. Note the tight distribution of stiffness measurements for each individual. The median and maximum coefficients of variation were 1.71% and 3.07%, respectively.

In the AD study, MRE demonstrated a significant difference in the brain stiffness of AD subjects compared to age- and gender-matched controls (Fig. 2). The median stiffness of the CN− group was 2.37 kPa (range: 2.17–2.62 kPa, $n = 14$), the median stiffness of the CN+ group was 2.32 kPa (range: 2.18–2.67 kPa, $n = 7$), and the median stiffness of the AD group was 2.20 kPa (range: 1.96–2.29 kPa, $n = 7$) ($P = 0.0055$, Kruskal–Wallis). Pairwise comparisons with the Wilcoxon rank sum test indicated that both the CN− group ($P = 0.0015$) and the CN+ group ($P = 0.026$) were significantly different from the AD group. The CN− and CN+ groups did not differ from each other ($P = 0.85$). Example magnitude images, wave images, and stiffness maps from an AD subject and an age-matched CN− subject are shown in Fig. 3 and a movie of animated wave images can be seen in Supporting Video 1, available online.

These results demonstrate that MRE can noninvasively measure changes in the mechanical properties of the human brain due to AD (Fig. 2). The average CSF content within the ROI of each subject did not differ between the three groups ($P = 0.62$, Kruskal–Wallis) and was less than 2% of the ROI on average, ensuring that the stiffness change results from a change in the mechanical properties of the brain parenchyma and is not a reflection of CSF volume change due to atrophy.

DISCUSSION

This work demonstrates that 3D brain MRE using a soft pillow driver, single-shot, spin-echo EPI pulse sequence and 3D DI algorithm is highly reproducible, and patients with AD have significantly softer brain

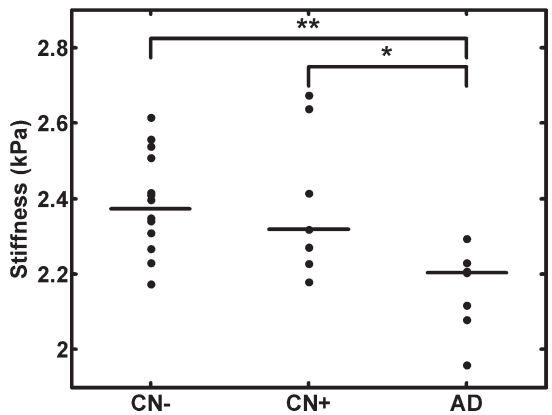

Figure 2. Plot of the median stiffness for each volunteer. Lines indicate the median stiffness of each group. The AD group had a significantly lower median stiffness than the CN− group (**$P = 0.0015$) and the CN+ group (*$P = 0.026$).

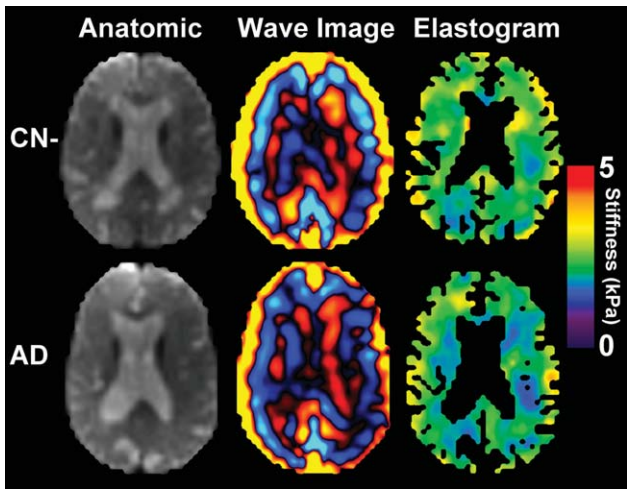

Figure 3. Example brain MRE images collected with a spin-echo EPI pulse sequence (axial plane, TR/TE = 1500/61.3 msec). Images in the top row show the results from an 89-year-old male CN– subject and the bottom row shows results from a 93-year-old male subject with AD. EPI magnitude images for each subject are shown in the first column. The second column shows the first time offset of the z component of the curl of the MRE wave images. The resulting elastograms are shown in the last column.

parenchyma than matched control subjects. The soft vibration source has proven reliable and comfortable. Other MRE driver technologies have been implemented for brain MRE and have demonstrated success for imaging normal subjects and patients with conditions such as multiple sclerosis and hydrocephalus (10–17). The ergonomic flexible driver used in this study provides good mechanical coupling by conforming to the head, thus generating a uniform and reproducible shear wave field. The vibration generated by this device was well tolerated, even in AD patients who displayed moderate disorientation. A concern raised during the reproducibility study was the abrupt transition from rest to full motion that could potentially lead to subject motion due to a startle response. To deal with this, a progressive ramping of the power from rest to full power over an 8-second period before the data were acquired was incorporated into the AD study. In addition, following the reproducibility study it was concluded that a 60-Hz vibration was more comfortable than the original choice of 55 Hz. So, as an additional measure to enhance the comfort of the exam for our subjects, we incorporated the 60 Hz frequency into the AD study.

The 3D brain MRE protocol evaluated in this work was shown to be highly reproducible in a cohort of 10 normal volunteers. The implementation of an accelerated spin-echo EPI MRE sequence at 3T allows for a fast acquisition of the 3D wave field. The algorithm utilized for calculating the curl of the wave data removes unwanted longitudinal and geometric wave effects (18) while also avoiding potential pitfalls of 3D phase unwrapping. The resulting curl images yielded reproducible inversions with a coefficient of variation less than 3.1%.

These stiffness measurements in healthy volunteers are in agreement with current MRE literature. Sack et al (14) have reported a mean brain shear modulus of 1.56 + 1.07i kPa at 50 Hz in six normal volunteers with comparable reproducibility to the work presented here. This complex shear modulus equates to a shear stiffness of 2.07 kPa (9). Although their work was done in 2D, they completed a full evaluation of their experimental setup to demonstrate that a 2D analysis should be sufficient to obtain an accurate stiffness inversion (11). At a higher frequency of 90 Hz and using a 3D direct inversion algorithm, Green et al (10) reported that white matter had a shear modulus of 2.7 + 2.5i kPa for five volunteers, equating to a shear stiffness of 4.24 kPa. As expected, the average of the 10 volunteers in this work, 3.07 kPa, lies between the work done at 50 and 90 Hz due to the dispersive and viscoelastic nature of brain tissue. Previous work by Kruse et al (12), however, reported higher brain stiffness values than the work outlined above. This discrepancy likely exists because this work was performed at a higher frequency (100 Hz) and only used a 2D acquisition and inversion that may not have been optimized to minimize through-plane wave propagation. Through-plane propagating waves can appear in 2D data as waves with longer wavelengths, thus overestimating the stiffness of the tissue. The difference in stiffness observed between the 10 volunteers in the reproducibility study (3.07 kPa at 55 Hz) and the 14 CN– subjects in the AD study (2.37 kPa at 60 Hz) is expected due to their age difference (15).

Decreased brain stiffness was demonstrated with MRE in this group of AD patients compared to the age- and gender-matched control subjects. The fact that our patients were demented indicates that they were all at a stage in the AD process where significant neurodegeneration had occurred, and that the entire AD pathological cascade had been engaged. Current thinking concerning AD pathogenesis is that the initial molecular events center on dysregulation of the processing of amyloid precursor protein leading to an increase in production of amyloidogenic β-amyloid-42 (Aβ). Aβ oligomerizes to form toxic fibrils leading to formation of the amyloid plaques that are a pathological hallmark of the disease. Downstream pathological events include dysregulation of tau kinases leading to neurofibrillary tangles (the second pathological hallmark of AD), oxidative stress, and finally synaptic loss, cell death, and dementia (19). Currently, biomarkers exist to assess Aβ load (PIB imaging (6) or CSF Aβ42), neurofibrillary tangles (CSF tau), synaptic dysfunction ([18F]fluoro-2-D-glucose positron emission tomography [FDG PET]), and neurodegeneration (structural MRI). The magnitude and rate of change of several biomarkers can be combined to determine the grade of an individual's disease (20).

Throughout the AD cascade, several processes may impact the mechanical properties of brain parenchyma. The amyloid fibrils themselves are six orders of magnitude greater in stiffness than neurons and glia (21,22). As a result, initially it seemed counterintuitive that global brain stiffness decreases due to AD. One hypothesis was that the aggregation of these stiff proteins containing β-pleated sheets would lead to an increase in the global brain stiffness. Not only did the

AD group demonstrate decreased brain stiffness, but the CN+ group was not different from the CN− group, indicating that the presence of brain amyloid alone is not responsible for the observed change in brain stiffness.

On the other hand, the decrease in stiffness may reflect a host of microstructural events that destroy normal cytoarchitectural integrity, such as degradation of the extracellular matrix following the deposition of hydrophobic amyloid protein, cytoskeletal disruption downstream of tau hyperphosphorylation, and loss of the interconnecting synaptic networks. Attributing the MRE findings to disease-related loss of microstructural integrity is consistent with well-established findings of increased mean diffusivity and decreased fractional anisotropy in AD on diffusion imaging (23,24). Figure 3 illustrates that the loss of brain stiffness in AD relative to CN is not limited to the cortex (which is where amyloid plaques are located) but also involves white matter.

In addition to the determination of decreased brain stiffness due to AD presented in this work, Wuerfel et al (17) utilized MRE to report decreased brain stiffness due to multiple sclerosis and Streitberger et al (16) reported decreased brain stiffness in patients with normal pressure hydrocephalus. While these results may suggest that MRE is an unspecific exam, it does have potential to improve the sensitivity of diagnosis for several diseases when used in the context of a patient's clinical background. For example, prolonged T2 relaxation is often an unspecific finding in a pathological process, yet it is a useful MR feature in diagnosing many neurological diseases.

In conclusion, we have demonstrated that 3D brain MRE can be performed reproducibly, and that AD pathology alters the mechanical properties of brain in a way that can be measured in vivo by MRE. MRE is a relatively new imaging modality that provides a unique class of information which heretofore has not been applied to AD. Measures of brain elasticity should provide unique insights into fundamental ultrastructural alterations of the brain that occur in AD, as well as how these change with time, correlate with other disease biomarkers, and with clinical expression of the disease.

ACKNOWLEDGMENTS

The authors thank Dr. Jun Chen for development of the soft driver, Scott Kruse for technical development, and Diane Sauter for performing the clinical examinations.

REFERENCES

1. McKhann G, Drachman D, Folstein M, Katzman R, Price D, Stadlan EM. Clinical diagnosis of Alzheimer's disease: report of the NINCDS-ADRDA Work Group under the auspices of Department of Health and Human Services Task Force on Alzheimer's Disease. Neurology 1984;34:939–944.
2. Hebert LE, Scherr PA, Bienias JL, Bennett DA, Evans DA. Alzheimer disease in the US population. Arch Neurol 2003;60:1119–1122.
3. Muthupillai R, Lomas DJ, Rossman PJ, Greenleaf JF, Manduca A, Ehman RL. Magnetic resonance elastography by direct visualization of propagating acoustic shear waves. Science 1995;269:1854–1857.
4. Yin M, Talwalkar JA, Glaser KJ, et al. Assessment of hepatic fibrosis with magnetic resonance elastography. Clin Gastroenterol Hepatol 2007;5:1207–1213.
5. Jack CR, Lowe VJ, Senjem ML, et al. ^{11}C PiB and structural MRI provide complimentary information in imaging of Alzheimer's disease and amnestic mild cognitive impairment. Brain 2008;131:665–680.
6. Klunk WE, Engler H, Nordberg A, et al. Imaging brain amyloid in Alzheimer's disease with Pittsburgh compound-B. Ann Neurol 2004;55:306–319.
7. Glaser KJ, Ehman RL. MR elastography inversions without phase unwrapping. In: Proc 17th Annual Meeting ISMRM, Honolulu; 2009:4669.
8. Romano AJ, Bucaro JA, Ehman RL, Shirron JL. Evaluation of a material parameter extraction algorithm using MRI-based displacement measurements. IEEE Trans Ultrason Ferroelectr Freq Control 2000;47:1575–1581.
9. Manduca A, Oliphant TE, Dresner MA, et al. Magnetic resonance elastography: non-invasive mapping of tissue elasticity. Med Image Anal 2001;5:237–254.
10. Green MA, Bilston LE, Sinkus R. In vivo brain viscoelastic properties measured by magnetic resonance elastography. NMR Biomed 2008;21:755–764.
11. Hamhaber U, Sack I, Papazoglou S, Rump J, Klatt D, Braun J. Three-dimensional analysis of shear wave propagation observed by in vivo magnetic resonance elastography of the brain. Acta Biomater 2007;3:127–137.
12. Kruse SA, Rose GH, Glaser KJ, et al. Magnetic resonance elastography of the brain. Neuroimage 2008;39:231–237.
13. Latta P, Gruwel MLH, Debergue P, Matwiy B, Sboto-Frankenstein UN, Tomanek B. Convertible pneumatic actuator for magnetic resonance elastography of the brain. Magn Reson Imaging 2011;29:147–152.
14. Sack I, Beierbach B, Hamhaber U, Klatt D, Braun J. Non-invasive measurement of brain viscoelasticity using magnetic resonance elastography. NMR Biomed 2008;21:265–271.
15. Sack I, Beierbach B, Wuerfel J, et al. The impact of aging and gender on brain viscoelasticity. Neuroimage 2009;46:652–657.
16. Streitberger K-J, Wiener E, Hoffmann J, et al. In vivo viscoelastic properties of the brain in normal pressure hydrocephalus. NMR Biomed 2010 [Epub ahead of print].
17. Wuerfel J, Paul F, Beierbach B, et al. MR-elastography reveals degradation of tissue integrity in multiple sclerosis. Neuroimage 2010;49:2520–2525.
18. Baghani A, Salcudean S, Rohling R. Theoretical limitations of the elastic wave equation inversion for tissue elastography. J Acoust Soc Am 2009;126:1541–1551.
19. Hardy J, Selkoe DJ. The amyloid hypothesis of Alzheimer's disease: progress and problems on the road to therapeutics. Science 2002;297:353–356.
20. Jack CR, Knopman DS, Jagust WJ, et al. Hypothetical model of dynamic biomarkers of the Alzheimer's pathological cascade. Lancet Neurol 2010;9:119–128.
21. Lu YB, Franze K, Seifert G, et al. Viscoelastic properties of individual glial cells and neurons in the CNS. Proc Natl Acad Sci U S A 2006;103:17759–17764.
22. Smith JF, Knowles TP, Dobson CM, MacPhee CE, Welland ME. Characterization of the nanoscale properties of individual amyloid fibrils. Proc Natl Acad Sci U S A 2006;103:15806–15811.
23. Kantarci K, Jack CR Jr, Xu YC, et al. Mild cognitive impairment and Alzheimer's disease: regional diffusivity of water. Radiology 2001;219:101–107.
24. Salat DH, Tuch DS, van der Kouwe AJW, et al. White matter pathology isolates the hippocampal formation in Alzheimer's disease. Neurobiol Aging 2010;31:244–256.